The Gaussian Noise Model in the Presence of Inter-Channel Stimulated Raman Scattering

Daniel Semrau, *Student Member, IEEE*, Robert I. Killey, *Senior Member, IEEE*, and Polina Bayvel, *Fellow, IEEE, Fellow, OSA*

***Abstract*—A Gaussian noise (GN) model, precisely accounting for an arbitrary frequency dependent signal power profile along the link, is presented. This allows accurate evaluation of the impact of inter-channel stimulated Raman scattering (ISRS) on the optical Kerr nonlinearity. Additionally, the frequency dependent fiber attenuation can be taken into account and transmission systems that use hybrid amplification schemes can be modeled, where distributed Raman amplification is partly applied over the optical spectrum. For the latter two cases, a set of coupled ordinary differential equations must be numerically solved to obtain the signal power profile yielding a semianalytical model. However for lumped amplification and negligible variation in fiber attenuation, a less complex and fully analytical model is presented denoted as the analytical ISRS GN model. The derived model is exact to first-order for Gaussian modulated signals and extensively validated by numerical split-step simulations. A maximum deviation of only 0.1 dB in nonlinear interference power between simulations and the ISRS GN model is reported. The model is applied to a transmission system that occupies the entire C + L band (10 THz optical bandwidth). At optimum launch power, changes of up to 2 dB in nonlinear interference power due to ISRS are reported. The ISRS GN model is quantitatively compared with other models published in the literature and found to be significantly more accurate.**

***Index Terms*—C + L band transmission, first-order perturbation, gaussian noise model, nonlinear interference, nonlinear distortion, optical fiber communications, stimulated raman scattering.**

I. Introduction

ANALYTICAL models that predict the performance degradation in optical fiber communications due to Kerr nonlinearity have become widespread in recent years. Most approaches analytically solve the nonlinear Schrödinger equation using a first-order perturbation approach with respect to the nonlinearity coefficient. The resulting expressions offer unique insight into the underlying parameter dependencies and are key enablers of efficient system design [1], rapid achievable rate estimations of point-to-point links [2]–[4] and physical layer aware network optimization. The latter is essential for optical network abstraction and virtualization leading to optimal and intelligent techniques to maximize optical network capacity [5]. Analytical models also offer a significant reduction in computational complexity with minor inaccuracies compared to split-step simulations and experiments [6]–[11].

The literature offers a wide range of analytical models varying in accuracy and complexity [12]–[23]. The first approaches in the context of modern coherent receivers and dispersion uncompensated links date back to 1993 and 2002 [12], [13], enabling the computation of the perturbation caused by Kerr nonlinearity. Similar results were independently derived by other groups and the model became widely known as the Gaussian noise (GN) model [14]–[16], [22], [24]. A key assumption of the works is the signal Gaussianity assumption, which is that the signal can be written as a Gaussian process at the fiber input. As a result of this assumption, the GN model relies on large accumulated dispersion [20, Section 6] and signals with high cardinality [19, Section 4], two conditions that are satisfied in most cases of modern coherent fiber communication.

The popularity of the GN model is undoubtledly due to its relative simplicity. However, as a result, it fails to predict certain properties of nonlinear interference (NLI) such as modulation format dependence [17]–[19], symbol rate dependence [25]–[29], nonlinear phase noise [19], [30], long temporal correlations [18], [19] and the dependence on the memory length of the fiber-optic channel [31]. In order to account for those properties, significantly more complex models have been proposed [17]–[21]. Comprehensive overviews can be found in [32], [33].

The impact of these, unaccounted for, properties is usually small for lumped, dispersion unmanaged, multi-span systems that use high-order modulation formats and the GN model can be considered sufficiently accurate. Additionally, modern optical transmission systems make use of probabilistically shaped constellations which increases the prediction accuracy [34]. Recently, the conventional GN model was experimentally validated for the central channel and optical bandwidths of up to 7.3 THz with a deviation of only 0.4 dB in nonlinear interference power [6], [35].

An assumption of all above-mentioned works is that every frequency component experiences the same power evolution along the link. They are, therefore, inaccurate in the prediction of ultra-wideband transmission systems where the variation of the fiber attenuation is not negligible and for bandwidths where inter-channel stimulated Raman scattering (ISRS) is significant.

Manuscript received January 7, 2018; revised March 9, 2018 and April 11, 2018; accepted April 23, 2018. Date of publication April 27, 2018; date of current version June 8, 2018. This work was supported in part by a UK EPSRC programme under Grant UNLOC EP/J017582/1 and in part by a Doctoral Training Partnership (DTP) studentship for Daniel Semrau. *(Corresponding author: Daniel Semrau.)*

The authors are with the Optical Networks Group, University College London, London WC1E 7JE, U.K. (e-mail: uceedfs@ucl.ac.uk; r.killey@ucl.ac.uk; p.bayvel@ucl.ac.uk).

Color versions of one or more of the figures in this paper are available online at http://ieeexplore.ieee.org.

Digital Object Identifier 10.1109/JLT.2018.2830973

Inter-channel stimulated Raman scattering is a non-parametric nonlinear process that amplifies low frequency components at the expensive of high frequency components within the same optical signal. In modern optical communications that use coherent technology in combination with dispersion-uncompensated fiber links, ISRS effectively introduces a different power profile for each frequency component [36]–[38]. For C band transmission (approximately 5 THz), as defined from the availability of the erbium doped fiber amplifier (EDFA), ISRS is not significant and its impact is negligible in most cases. However, for systems that occupy the entire C + L band (approximately 10 THz) or beyond, ISRS becomes significant and it must be taken into account. Beyond C + L band transmission could be enabled by lumped Raman amplification or the use of other dopants such as bismuth [39] or quantum dots in semiconductor amplifiers [40] [41].

The first approach to include ISRS in the GN model was published in [42]. The authors approximated the signal power profile with an exponential decay using an effective attenuation coefficient that matches the (frequency dependent) effective length in the presence of ISRS. Although enabling initial conclusions on the impact of ISRS, there are two shortcommings of this approach. First, when ISRS is significant, the resulting signal power profile does not resemble an exponential decay, particularly in the beginning of the fiber span, where Kerr nonlinearity prevails. Second, the work assumes that, during the four-wave mixing (FWM) process, every participating frequency component attenuates in the same manner as the channel of interest. In other words, for the induced nonlinear perturbation at frequency f, every frequency component in the triplet (f, f_1, f_2) attenuates as f during the nonlinear mixing. Therefore, this approach overestimates the impact of ISRS on the Kerr nonlinearity and ISRS is not accurately taken into account.

A more rigorous approach to include ISRS in the GN model was published in [43]–[45]. In all three works, the channel under test (i.e., frequency component f) attenuates precisely according to the signal power profile $g(f)$ resulting from ISRS (or any arbitrary profile), lifting the exponential decay assumption in [42]. However, for an attenuation profile that is linear in frequency (like the one resulting from ISRS), the frequencies in the triplet (f, f_1, f_2) also attenuate according to f during the FWM process. Therefore, this approach overestimates the impact of ISRS on the Kerr nonlinearity and the frequency dependent signal power profile is not accurately taken into account.

In this paper, a Gaussian noise model, accounting for any arbitrary frequency dependent signal power profile, is described. This enables the modeling of nonlinear interference in ultra-wideband regimes where ISRS is significant. The model is refered to as the ISRS GN model throughout this paper. Additionally, the variation in fiber attenuation and hybrid amplification schemes can be included. In general, the signal power profile is obtained by numerically solving a set of coupled ordinary differential equations (ODE). This yields a semi-analytical ISRS GN model which relies on a numerical ODE solver.

However, for lumped amplification and negligible variation in fiber attenuation, a fully analytically model is derived based on a linear approximation on the ISRS gain function. This reduces model as well as computational complexity. The analytical ISRS GN model holds for bandwidths up to approximately 14 THz after which the Raman gain function cannot be considered linear anymore.

This paper is organized as follows. In Section II, the ISRS GN model is presented and its key derivation steps are briefly outlined. The detailed derivation can be found in the Appendix A. The model is extensively validated by split-step simulations in Section III and applied to a C + L band transmission system based on standard single mode fiber (SMF) spans in Section IV. In Sections III and IV, the results in [42]–[45] are benchmarked against the ISRS GN model.

II. The ISRS GN Model

In order to maximize the information throughput of an optical communication system, it is vital to evaluate and maximize the performance of each individual channel that is transmitted. After coherent detection and electronic dispersion compensation, the channel dependent signal-to-noise ratio (SNR) can be calculated as

$$\mathrm{SNR}_i \approx \frac{P_i}{P_{\mathrm{ASE}} + \eta_n P_i^3}, \tag{1}$$

where P_i is the launch power of channel i, P_{ASE} is the accumulated amplified spontaneous emission (ASE) noise power at the receiver and η_n is the nonlinear interference coefficient after n spans. The SNR is a function of the spectral location of the channel within the optical signal as P_{ASE} and η_n are frequency dependent quantities. When the channel bandwidth B_{ch} is small compared to the total optical bandwidth B and the spectral gaps between adjacent channels are sufficiently small, the power spectral density (PSD) of the NLI can be considered locally flat and η_n can be approximated as

$$\eta_n(f_i) = \int_{-\frac{B_{\mathrm{ch}}}{2}}^{\frac{B_{\mathrm{ch}}}{2}} \frac{G(\nu + f_i)}{P_i^3} d\nu \approx \frac{B_{\mathrm{ch}}}{P_i^3} G(f_i), \tag{2}$$

where f_i is the center frequency of channel i and $G(f)$ is the PSD of the nonlinear interference. For later use, we further define the total optical launch power as

$$P_{\mathrm{tot}} = \int G_{\mathrm{Tx}}(\nu) d\nu = \sum_{\forall i} P_i, \tag{3}$$

where G_{Tx} is the input PSD of the entire optical signal. The aim of the next sections is to find an analytical expression for the nonlinear interference PSD $G(f)$, in order to compute the channel dependent SNR or similar performance metrics.

A. The Nonlinear Interference Power

Various models have been proposed in the past in order to calculate the NLI power, where it is generally assumed that all frequency components attenuate in the same manner along a fiber span [12]–[24]. However, this assumption is no longer satisfied when transmission systems operate at large optical bandwidths (C + L band and beyond). This is because each frequency component undergoes a different power evolution during propagation as a result of ISRS and a frequency dependent attenuation

coefficient. In addition, frequency dependent signal power profiles are present in hybrid amplification schemes, where part of the spectrum is amplified using distributed Raman amplifiers in order to reduce the ASE noise power for longer wavelengths or to extend the amplification window beyond conventional EDFAs [46]–[48].

For a frequency dependent power evolution, the PSD of the NLI after one span is derived in Appendix A and it is found to be

$$G(f) = \frac{16}{27}\gamma^2 \int df_1 \int df_2\, G_{\mathrm{Tx}}(f_1) G_{\mathrm{Tx}}(f_2) G_{\mathrm{Tx}}(f_1+f_2-f) \cdot \left| \int_0^L d\zeta \sqrt{\frac{\rho(\zeta, f_1)\rho(\zeta, f_2)\rho(\zeta, f_1+f_2-f)}{\rho(\zeta, f)}} e^{j\phi(f_1, f_2, f, \zeta)} \right|^2, \tag{4}$$

where $\phi = -4\pi^2(f_1 - f)(f_2 - f)\left[\beta_2 + \pi\beta_3(f_1 + f_2)\right]\zeta$, β_2 is the group velocity dispersion (GVD) parameter, β_3 is the linear slope of the GVD parameter, γ is the nonlinearity coefficient and $\rho(z, f)$ is the normalized signal power profile. For example, the normalized signal power profile of a passive fiber with constant attenuation coefficient α is $\rho(z, f) = e^{-\alpha z}$. For multi-span systems, where each span has identical fiber parameters and signal power profiles, the phased-array term

$$\chi(f_1, f_2, f) = \left| \frac{\sin\left[\frac{1}{2} n \phi(f_1, f_2, f, L)\right]}{\sin\left[\frac{1}{2}\phi(f_1, f_2, f, L)\right]} \right|^2 \tag{5}$$

must be inserted into the integral in (4). For multi-span systems with non-identical signal power profiles for each span (e.g., when non-ideal gain flattening filters are considered), the phased-array term cannot be used. This is particularly important for hybrid amplification schemes where multiple pumps are used which are usually optimized to deliver uniform gains across the optical spectrum [49]. In order to account for non-identical multi-span systems, (4) must be used, where L must be reinterpreted as the link length and $\rho(z, f)$ as the signal power profile for the *entire* link. For simplicity, identical spans are considered for the remainder of this work.

We note that (4) is different than the result derived in [43, Eq. (16)], [44, Eq. (18)] and [45, Eq. (1)], where $\rho(\zeta, f_1 + f_2 - f)$ and $\rho(\zeta, f)$ are swapped.[1] However, in Section III, it is shown by split-step simulations that (4) is the correct formula.

Eq. (4) can be used to model any arbitrary frequency dependent signal power profile and it is therefore suitable to evaluate the impact of ISRS on the optical Kerr nonlinearity.

[1] As a consequence of the different result, the f_1 and f_2 dependence vanishes, for power profiles of the form $\rho(z, f) = e^{a(z)\cdot f + b(z)}$ (as the one resulting from ISRS). This means that in the nonlinear process all three frequencies in the triplet (f, f_1, f_2) attenuate according to frequency f which overestimates the impact of ISRS. In contrast, in (4) each frequency (f_1, f_2, f) correctly attenuates with ist respective power profile.

During the peer-review process of this manuscript, two papers have appeared, namely an update of [44] and [50] as well as an erratum [51]. The update of [44] was a direct response to the arXiv e-print version of this manuscript [52], correcting [44, Eq. (1)] with the correct expression (4), first published in [52]. Erratum [51] corrected the same error in [43, Eq. (16)] and was also submitted following the publication of [52].

B. Inter-channel Stimulated Raman Scattering

In the following, the PSD of the NLI in the presence of ISRS is presented, which is hereafter referred to as the ISRS GN model. Inter-channel stimulated Raman scattering can be separated into two effects, namely an average ISRS gain component and a time dependent cross talk component. This time dependent cross talk is responsible for gain fluctuations and relative-intensity-noise (RIN) transfer like effects, which are commonly found in distributed Raman amplifiers. In the context of ISRS and high dispersive links, the gain fluctuations are significantly reduced and can be typically neglected as they are averaged between many independently modulated channels as theoretically shown in [36]–[38]. Recently, the negligibility of the time dependent cross talk has been experimentally demonstrated [53], [54]. Similar observations have been made in the context of distributed Raman amplification [55].

The resulting (average) frequency dependent signal power profile can be obtained by solving a set of coupled ordinary differential equations [56, Eq. (3)]

$$\frac{\partial P_i}{\partial z} = \underbrace{-\sum_{k=i+1}^{M} \frac{f_k}{f_i} g_{\mathrm{r}}(\Delta f) P_k P_i}_{\text{ISRSloss}} + \underbrace{\sum_{k=1}^{i-1} g_{\mathrm{r}}(\Delta f) P_k P_i}_{\text{ISRSgain}} - \alpha(f_i) P_i, \tag{6}$$

where M is the total number of WDM channels, $g_r(\Delta f)$ is the polarization averaged, normalized (by the effective core area A_{eff}) Raman gain spectrum for a frequency separation $\Delta f = |f_i - f_k|$ and $\alpha(f)$ is the frequency dependent attenuation coefficient. The index of the channel with the highest center frequency is $i = 1$. (6) can be extended to include distributed Raman amplification using [57, Eq. 1]. (6) has no general analytical solution and must be solved numerically. The obtained power profile can then (after normalization) be inserted in (4) to yield a semi-analytical ISRS GN model that accurately accounts for ISRS, a frequency dependent attenuation coefficient and distributed Raman amplification.

The variation of the attenuation coefficient typically does not exceed 0.01 dB/km across the C + L band ranging from 1530 nm to 1625 nm and might be negligible depending on accuracy and computational complexity requirements [58]. The impact of a frequency dependent attenuation on the NLI coefficient can be loosely upper bounded by assuming that *every* frequency component attenuates according to the minimum in one case and according to the maximum attenuation coefficient in another case. The resulting maximum deviation in NLI coefficient is then

$$\Delta\eta_1\,[\mathrm{dB}] < \left(\frac{\alpha_{\min}}{\alpha_{\max}}\right)[\mathrm{dB}], \tag{7}$$

where $(\cdot)\,[\mathrm{dB}]$ means conversion to decibel and $\alpha_{\min}$ and $\alpha_{\max}$ is the minimum and maximum attenuation coefficient, respectively. In (7) it was assumed that $e^{-\alpha L} \ll 1$, $\ln\left(\pi^2 B^2 |\beta_2|/\alpha_{\min}\right) \approx \ln\left[\pi^2 B^2 |\beta_2|/\alpha_{\max}\right]$ and [59, Eq. 5] was

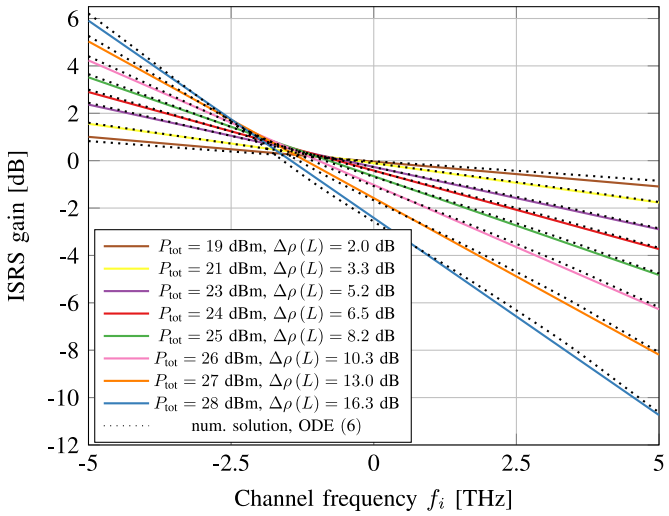

Fig. 1. The gain over 100 km transmission due to ISRS as a function of channel frequency obtained by solving the set of coupled differential equations (6) shown in dotted lines and its analytical triangle approximation (8) shown in solid lines for a variety of total optical launch powers P_{tot}. The power difference of the outer channels after transmission is denoted as $\Delta\rho\,(L)$.

used. For an attenuation deviation of 0.01 dB/km over 95 nm, (7) yields a maximum deviation of only $\Delta\eta_1$ [dB] < 0.2 dB.

This contribution may be deemed negligible and the prevailing effect that causes a frequency dependent signal power profile is inter-channel stimulated Raman scattering.

Eq. (6) can then be solved analytically when the Raman gain spectrum is assumed to be linear up to approximately 14 THz (i.e., up to the Stokes shift). The normalized signal power profile for a spectral component f is then given by [60, Eq. (7)]

$$\rho(z,\, f) = \frac{P_{\text{tot}} e^{-\alpha z - P_{\text{tot}} C_{\text{r}} L_{\text{eff}} f}}{\int G_{\text{Tx}}(\nu) e^{-P_{\text{tot}} C_{\text{r}} L_{\text{eff}} \nu} d\nu}, \tag{8}$$

where C_{r} is the slope of a linear regression of the normalized Raman gain spectrum $g_r(\Delta f)$ and $L_{\text{eff}} = \frac{1-\exp(-\alpha z)}{\alpha}$. The z dependence in L_{eff} is suppressed for notational convenience. The linear approximation of the Raman gain spectrum is often referred to as triangular approximation.

The ISRS gain of a 10 THz signal after 100 km propagation, obtained by numerically solving (6) using the Raman gain spectrum as in [61] and its analytical approximation (8) are shown in Fig. 1. The precise functions that have been used can be found in [42, Fig. 1]. For a relatively high optical launch power of 28 dBm, the average deviation between the numerical solution and its approximation is 0.18 dB which can be considered negligible. Therefore, the analytical solution (8) is sufficiently accurate for modeling the nonlinear interference power.

Substituting (8) in (4) yields the reference formula of the analytical ISRS GN model as

$$G(f) = \frac{16}{27}\gamma^2 \int df_1 \int df_2\; G_{\text{Tx}}(f_1) G_{\text{Tx}}(f_2) G_{\text{Tx}}(f_1 + f_2 - f) \cdot \left| \int_0^L d\zeta \frac{P_{\text{tot}} e^{-\alpha\zeta - P_{\text{tot}} C_{\text{r}} L_{\text{eff}}(f_1+f_2-f)}}{\int G_{\text{Tx}}(\nu) e^{-P_{\text{tot}} C_{\text{r}} L_{\text{eff}} \nu} d\nu} e^{j\phi(f_1, f_2, f, \zeta)} \right|^2. \tag{9}$$

TABLE I
SYSTEM PARAMETERS

Parameters	**(a)**	**(b)**
for section	**III**	**IV**
Loss (α) [dB/km]	0.2	
Dispersion (D) [ps/nm/km]	17	
Dispersion slope (S) [ps/nm^2/km]	0	0.067
NL coefficient (γ) [1/W/km]	1.2	
Raman gain slope (C_{r}) [1/W/km/THz]		0.028
Raman gain ($C_{\text{r}} \cdot 14$ THz) [1/W/km]		0.4
Fiber length (L) [km]	100	
Symbol rate (B_{ch}) [GBd]	10	50
Channel spacing [GHz]	10.001	50.001
Number of channels	101	201
Optical bandwidth (B) [THz]	1.01	10.05
Roll-off factor [%]	0.01	
Number of symbols [2^x]	15	
Step size [m]	5	

Eq. (9) is a key result of this work which is extensively validated in Section III and further applied to a C + L band case study in Section IV. It should be noted that (9) is valid for arbitrary WDM spectra and is not restricted to the case of continuous input PSDs.

It is useful to analyze (8) in more detail. After trivial algebraic manipulations, we obtain that the power transfer between the outer channels can be computed as [60, Eq. (8)]

$$\Delta\rho\,(z)\,[\text{dB}] = 4.3 \cdot P_{\text{tot}} C_{\text{r}} L_{\text{eff}} B, \tag{10}$$

which is *independent* of the spectral distribution of the input power.

For modern fiber parameters $L_{\text{eff}} = 26$ km, $C_{\text{r}} = 0.008$ 1/W/km/THz (approximately corresponding to a Corning® Vascade® EX2000 fiber with $A_{\text{eff}} = 111$ μm) and a launch power of 2 dBm per 40 GBd channel, which maximizes the SNR of the central channel as in [6], an ISRS power transfer of $\Delta\rho = 1$ dB is present at a bandwidth of 5.3 THz and $\Delta\rho > 4$ dB for bandwidths larger than 10.6 THz.

III. NUMERICAL VALIDATION

In this section, the analytical ISRS GN model (9) is validated by split-step simulations for an optical fiber communication system with parameters listed in Table I(a). Numerically solving the Manakov equation for the entire C + L band (approximately 10 THz) is extremely challenging, due to high memory requirements and the excessive use of very large fast Fourier transforms.

Therefore, the validation was carried out over bandwidth, $B = 1$ THz with an artificially increased Raman gain slope C_{r}. Varying the Raman gain slope was necessary to yield significant power transfer over 1 THz. The considered power transfer values ranged from $\Delta\rho\,(L) = 0$ dB to $\Delta\rho\,(L) = 8.2$ dB corresponding to the ISRS gain shown in Fig. 1. The power transfer (8) was integrated into the split-step simulations by introducing a frequency dependent power profile at each simulation step.

The transmitted symbols were drawn from a circular-symmetric, complex Gaussian distribution in order to emulate the signal Gaussianity assumption of the GN model. Additionally, a small channel bandwidth was chosen such that $B \gg B_{\mathrm{ch}}$. The receiver consisted of digital dispersion compensation, ideal root-raised-cosine (RCC) matched filtering and constellation rotation. The SNR was ideally estimated as the ratio between the variance of the transmitted symbols $E[|X|^2]$ and the variance of the noise σ^2, where $\sigma^2 = E[|X - Y|^2]$ and Y represents the received symbols after digital signal processing. The nonlinear interference coefficient was then estimated via (1) and was compared with the predictions of the ISRS GN model via (2) and (9).

Ideal, noiseless amplifiers were considered to ease the NLI computation and the launch power was fixed to -1 dBm per channel. Additionally, a spectrally uniform launch power was assumed yielding

$$G_{\mathrm{Tx}}(f) = \frac{P_{\mathrm{tot}}}{B} \Pi\left(\frac{f}{B}\right), \tag{11}$$

for the model calculations, where $\Pi(x)$ denotes the rectangular function. A step size of 5 m was found to be sufficiently accurate for the given parameter. A further reduction of the step size resulted in a negligible change in SNR (< 0.01 dB).

The results for the nonlinear interference coefficient after one span as a function of the channel frequency f_i is shown in Fig. 2(a) and as a function of total launch power in Fig. 2(b). The accuracy of the ISRS GN model is remarkable with a maximum deviation of < 0.1 dB. The deviation is slightly higher at the exact spectral edges. At the exact spectral edges the NLI PSD varies over the channel bandwidth and the NLI PSD cannot be considered locally flat as in (2). This is not an inherit approximation of the ISRS GN model and it can be lifted by properly integrating over the NLI PSD. As expected, the ISRS GN model converges to the conventional GN model for negligible power transfer values. For stronger ISRS, the nonlinear interference PSD begins to tilt. The NLI is decreased for channels that experience net ISRS loss and increased for channels that experience net ISRS gain. Moreover, as shown in Fig. 2(b), the NLI coefficient depends exponentially on the ISRS power transfer. Fig. 2(b) indicates further that the ISRS dependence of the NLI coefficient is stronger for an increasing number of spans.

For Gaussian modulation, the NLI accumulation in decibels as a function of fiber spans can be written as [14, Section IX]

$$(\eta_n)\,[\mathrm{dB}] - (\eta_1)\,[\mathrm{dB}] = (1 + \epsilon) \cdot (n)\,[\mathrm{dB}], \tag{12}$$

where $(\cdot)\,[\mathrm{dB}]$ denotes conversion to decibel scale and ϵ is the coherence factor that is a measure for coherent accumulation of the NLI. As the coherence factor depends on the signal power profile (cf. [14, Fig. 10] and [11, Fig. 3]), it is affected by ISRS. The accumulation of NLI together with the resulting coherence factor obtained from the ISRS GN model and simulation results are shown in Fig. 3. Indeed, ISRS introduces a power dependent tilt on the coherent accumulation. This corresponds to the increasing power dependence of the NLI coefficient with increasing span number.

To benchmark our results against previous works, the results obtained using [43, Eq. (16)], [44, Eq. (18)] and [45, Eq. (1)] are shown in dashed in Fig. 2(a) using the same frequency dependent power profile (8). The difference originates due to the reason described in Section II-A, effectively assuming that all frequencies in the nonlinear process attenuate as the one that is evaluated (i.e., f_i). The deviation therefore increases with increasing ISRS gain towards outer channels.

The results obtained using the model in [42] is shown by dotted lines. The model implements the conventional GN model, where an effective attenuation coefficient is used, that matches the effective length of the evaluated channel f_i. Consequently, the frequency dependent attenuation within the nonlinear process is not properly accounted for, mainly resulting in an underestimation of the ISRS impact.

Based on the numerical validation carried out in this section, it is concluded that the ISRS GN model (9) accurately predicts the nonlinear interference resulting from inter-channel stimulated Raman scattering.

IV. C + L Band Transmission

In this section, the ISRS GN model is used to evaluate the impact of ISRS on a C + L band transmission system covering 10 THz of optical bandwidth with parameters listed in Table I(b). The considered uniform launch powers ranged from -13 dBm per channel ($P_{\mathrm{tot}} = 10$ dBm) to 5 dBm per channel ($P_{\mathrm{tot}} = 28$ dBm). Launch powers as high as 28 dBm were considered to quantify the impact of ISRS beyond typical power levels. There is strong evidence that this is still within the validity of the first-order perturbation approach. In the highly nonlinear regime, where the impact of ASE noise can be neglected, the SNR changes by at most -2 dB per 1 dBm increase in launch power, according to (1) and in the absence of ISRS. This is in agreement with experimental results for launch powers of at least up to 7 dBm per 40 GBd channel (4.1 THz optical bandwidth) [6, Fig. 4] and numerical results for launch powers of at least up to 4 dBm per 49 GBd channel (5 THz optical bandwidth) [23, Fig. 10].

The NLI coefficient as a function of channel frequency is shown in Fig. 4(a). For a particular launch power, the corresponding ISRS gains can be found in Fig. 1.

The tilt in NLI coefficient in the absence of ISRS is due to the dispersion slope S (or β_3), where lower frequencies experience a higher amount of dispersion and therefore experience reduced NLI. As the launch power is increased, the effect of ISRS starts to balance the effect of the dispersion slope in terms of NLI. At a launch power of 22 dBm, the NLI PSD is almost flat showing that ISRS and the dispersion slope are somewhat complementing each other in flattening the NLI spectrum. Assuming an EDFA noise figure of 5 dB, the uniform launch power that maximizes the SNR of the central channel is approximately 1 dBm ($P_{\mathrm{tot}} = 24$ dBm) in the absence of ISRS. It should be noted that a uniform total launch power of 24 dBm does not maximize the *overall* system performance. The value of 24 dBm only serves as

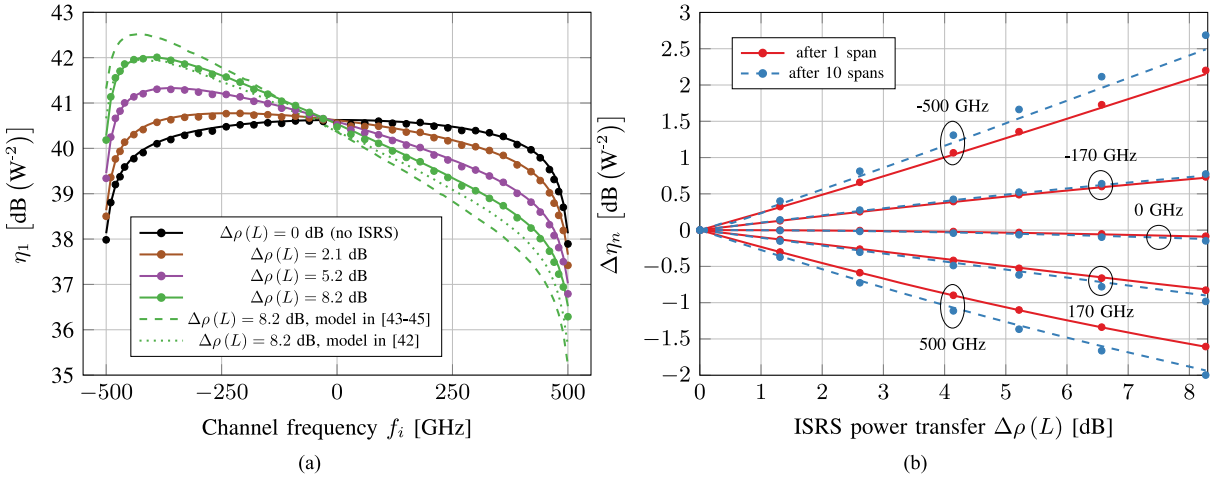

Fig. 2. The nonlinear interference coefficient after 1 span as a function of channel frequency is shown in (a) and the NLI change due to ISRS induced power transfer $\Delta\rho\,(L)$ is shown in (b). Solid lines represent the analytical ISRS GN model (9) and markers represent results obtained by split-step simulations. For comparison, the model in [42] is shown with a dotted line and the model in [43–45] is shown with a dashed line for an ISRS power transfer of $\Delta\rho = 8.2$ dB in (a). The power difference of the outer channels after transmission is denoted as $\Delta\rho\,(L)$.

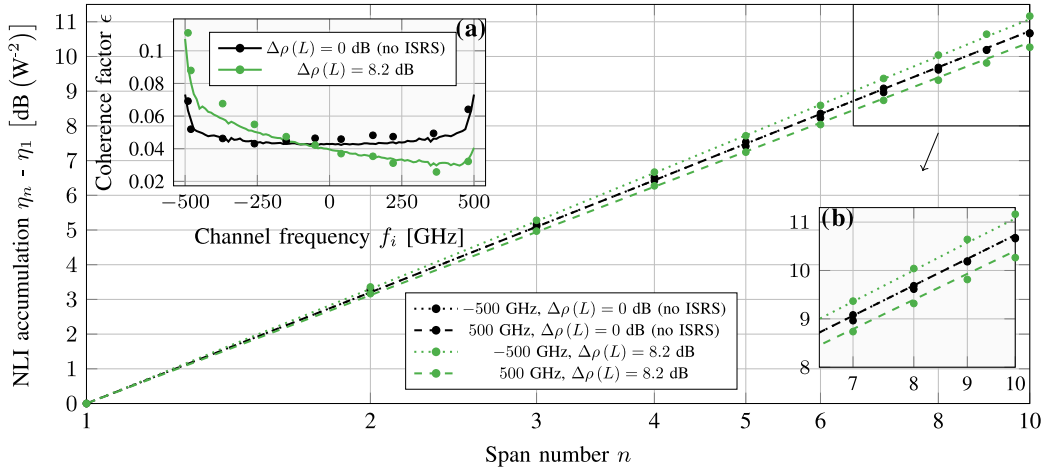

Fig. 3. The accumulation of NLI as a function of span number for the outer channels of the signal with and without ISRS. Lines represent the analytical ISRS GN model (9) and markers represent split-step simulations. The inset (a) shows the coherence factor after 10 spans and the inset (b) shows a magnified area of the figure.

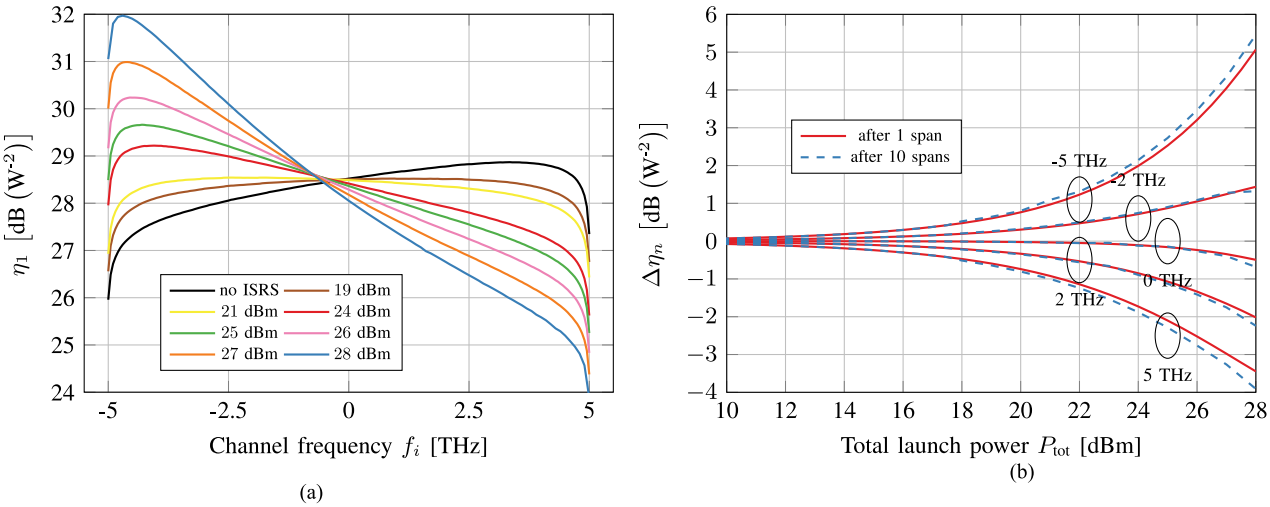

Fig. 4. The nonlinear interference coefficient after 1 span as a function of channel frequency for different total launch powers is shown in (a) and the NLI as a function of total launch power is shown in (b) obtained by the analytical ISRS GN model (9). The uniform launch power that maximizes the SNR for the central channel is 24 dBm, assuming a 5 dB EDFA noise figure.

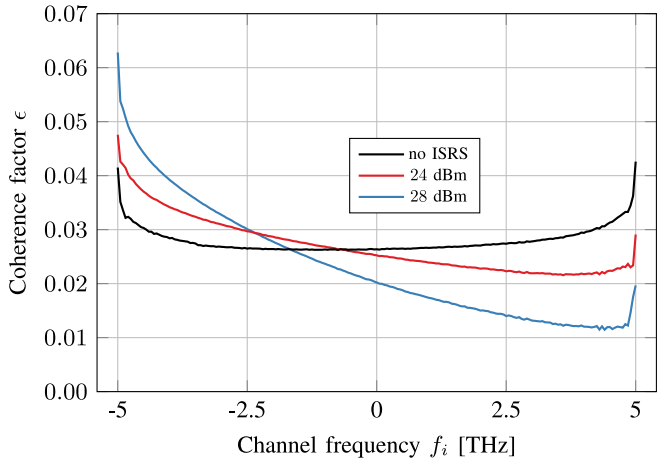

Fig. 5. The coherence factor as a function of channel frequency for a variety of total launch powers obtained by the analytical ISRS GN model (9).

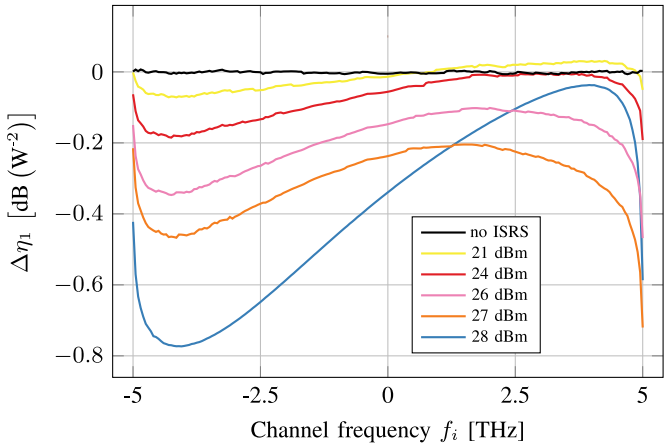

Fig. 6. Deviation of the NLI coefficient after one span between the analytical ISRS GN model (9) and [42]. The validity of the ISRS GN model is shown in Section III.

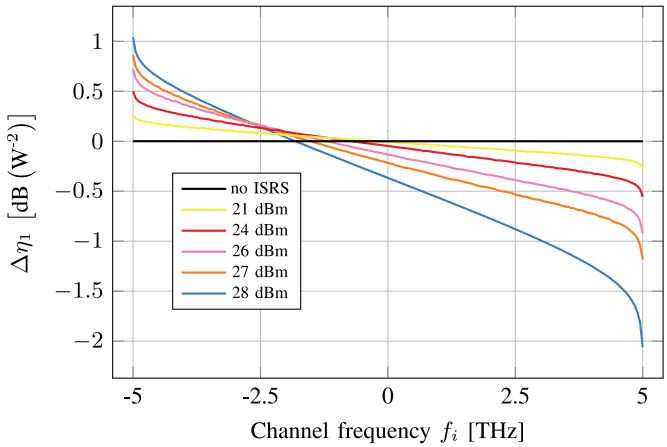

Fig. 7. Deviation of the NLI coefficient after one span between the analytical ISRS GN model (9) and [43]–[45]. The validity of the ISRS GN model is shown in Section III.

an approximate indicator for the expected ISRS power transfer of the studied system. At 24 dBm, the resulting ISRS power gain ranges from −3.7 dB to 2.9 dB while the resulting NLI deviation ranges from −1.7 dB to 2 dB over the transmitted spectrum.

The deviation of the NLI coefficient as a function of total launch power is shown in Fig. 4(b). The NLI PSD depends exponentially on the total launch power like the ISRS gain itself as already discussed in Section III. The deviation of the outer channels is 0.5 dB at 18 dBm launch power. In Section III it was shown that the coherence factor is changed as a result of ISRS. The same effect is seen in Fig. 4(b), where the deviation of the NLI is stronger for an increased number of spans.

The coherence factor as a function of channel frequency is shown in Fig. 5. The coherence factor is relatively small ($\epsilon < 0.07$) due to the large bandwidth. In the absence of ISRS the average coherence factor is 0.027. Using (12) the average coherent NLI accumulation $\epsilon \cdot (n)$ [dB] is 0.3 dB and 0.5 dB after 10 and 50 spans, respectively. For 24 dBm launch power, the maximum deviation in coherence factor is found to be 0.013 at the outer channels. This corresponds to a deviation in coherent NLI accumulation of 0.1 dB and 0.2 dB after 10 and 50 spans, respectively. The change in coherence factor due to ISRS might be deemed negligible depending on the accuracy requirements of the application.

To relate our work to previously published results, the NLI coefficient after one span obtained by the ISRS GN model is compared to the works [42] and [43]–[45]. The signal power profile as in (8) was used for all comparisons. The deviation of the NLI coefficient between the ISRS GN model and that of [42] is shown in Fig. 6. For 24 dBm launch power, the deviation stays below 0.19 dB. Even for high ISRS gains at 28 dBm launch power, the maximum deviation is 0.8 dB.

The deviation of the NLI coefficient between the ISRS GN model and [43, Eq. (13) and (16)], [44, Eq. (18)], [45, Eq. (1)] is shown in Fig. 7. The maximum deviation is 0.56 dB and 2.1 dB for 24 dBm and for 28 dBm launch power, respectively. The reader is referred to Sections II-A and III for the origin of the discrepancy.

Based on this analysis, it is concluded that the impact of ISRS on the Kerr nonlinearity is significant in C + L band systems. This is strongly dependent on launch power and the Raman gain slope due its exponential relationship to the nonlinear interference power. It should be noted that idealized gain flattening filters (GFF) were considered in this work to compensate the ISRS power transfer at the end of each span. When realistic GFF's are considered, the ISRS gain accumulates over distance and the impact on the nonlinear interference power is more significant than as shown in this section.

V. Conclusion

The ISRS GN model which analytically models the impact of inter-channel stimulated Raman scattering on the nonlinear perturbation caused by Kerr nonlinearity was proposed and analyzed in detail. Its accuracy was compared to split-step simulations and a maximum deviation of 0.1 dB in nonlinear interference power was found. The model can further account for the frequency dependent fiber attenuation, optical bandwidths beyond the Stokes shift (approximately 14 THz) and hybrid-

amplified transmission systems at the expense of greater computational complexity using a semi-analytical approach.

It was shown that ISRS changes the nonlinear interference power by up to 2 dB at optimum launch power for the studied C + L band transmission system. For such optical bandwidths and beyond, ISRS must be addressed in order to maximize system performance. Possible solutions in the physical layer include the use of gain flattening filters, optimized launch power distributions or tailored fiber designs, all of which can be modeled and analyzed using the results in this paper.

The derived ISRS GN model is, therefore, a powerful tool for efficient design, optimization, capacity calculations and physical-layer abstractions of ultra-wideband transmission systems that operate over the entire C + L band and beyond.

Appendix A
Derivation of the ISRS GN Model

In this section, (4) is derived for one span based on the nonlinear Schrödinger equation (NLSE) and a first-order regular perturbation approach. The result for one span can then be extended to multiple spans using the phased-array term (5) or reinterpreting a span as the entire link length with an according signal power profile. Instead of a constant attenuation coefficient α, a generic frequency and distance dependent gain coefficient $g(z, f)$ is used to model the effect of inter-channel stimulated Raman scattering. For the sake of brevity, only the key derivation steps are outlined.

We begin with the NLSE in the frequency domain which is given by [62, Ch. 2]

$$\frac{\partial}{\partial z}E(z,f) = \widetilde{\Gamma}(z,f)E(z,f) + j\gamma E(z,f) * E^*(z,-f) * E(z,f), \quad (13)$$

with $\widetilde{\Gamma}(z,f) = \frac{g(z,f)}{2} + j2\pi^2\beta_2 f^2 + j\frac{4}{3}\pi^3\beta_3 f^3$ and $u(x) * v(x)$ denoting the convolution operation. The complex envelope of the electric field $E(z, f)$ is expanded in a regular perturbation series with respect to the nonlinearity coefficient γ. The series is then truncated to first-order and we have

$$E(z,f) = E^{(0)}(z,f) + \gamma E^{(1)}(z,f). \quad (14)$$

Inserting (14) in (13), we obtain

$$E^{(0)}(z,f) = E(0,f)\cdot e^{\Gamma(z,f)}, \quad (15)$$

with $\Gamma(z,f) = \int_0^z \widetilde{\Gamma}(\zeta,f)\,d\zeta$ as the solution for the zeroth-order terms and a linear ordinary differential equation for the first-order terms as

$$\frac{\partial}{\partial z}E^{(1)}(z,f) = \widetilde{\Gamma}(z,f)E^{(1)}(z,f) + Q(z,f), \quad (16)$$

with $Q(z,f) = jE^{(0)}(z,f) * E^{(0)*}(z,-f) * E^{(0)}(z,f)$. The initial condition for the first-order solution is $E^{(1)}(0,f) = 0$ and we obtain

$$E^{(1)}(z,f) = e^{\Gamma(z,f)}\int_0^z \frac{Q(\zeta,f)}{e^{\Gamma(\zeta,f)}}d\zeta, \quad (17)$$

as the solution of (16).

In order to compute $Q(z, f)$, we assume that the input signal can be modeled as a periodic Gaussian process, a key assumption of the GN model, which is [24, Eq. 13]

$$E(0,f) = \sqrt{f_0 G_{\mathrm{Tx}}(f)}\sum_{n=-\infty}^{\infty}\xi_n\delta(f-nf_0), \quad (18)$$

where $G_{\mathrm{Tx}}(f)$ is the power spectral density of the input signal, ξ_n is a complex circular Gaussian distributed random variable, $T_0 = f_0^{-1}$ is the period of the signal and $\delta(x)$ denotes the Dirac delta function. For notational convenience, we write nf_0 as f_n and $\sum_{n=\infty}^{\infty}$ as $\sum_{\forall n}$ for the remainder of this derivation. Using (18), $Q(z, f)$ can be written as

$$Q(z,f) = jf_0^{\frac{3}{2}}\sum_{\forall m}\sum_{\forall n}\sum_{\forall k}\sqrt{G_{\mathrm{Tx}}(f_m)G_{\mathrm{Tx}}(f_n)G_{\mathrm{Tx}}(f_k)}\,\xi_m\xi_n^*\xi_k\delta(f-f_m+f_n-f_k)\,e^{\Gamma(z,f_m)+\Gamma^*(z,f_n)+\Gamma(z,f_k)}. \quad (19)$$

To first order, it can be shown that only non-degenerate frequency triplets in (19) contribute to the nonlinear interference power. Degenerate frequency triplets merely introduce a constant phase shift of the first-order solution $E^{(1)}(z, f)$, which cancels out when the PSD of $E^{(1)}(z, f)$ is computed. For more details, the reader is referred to [63, Ch. IV.B and IV.D]. Therefore, we neglect degenerate frequency triplets in order to keep the derivation concise. Similar to [63], we define the triplets of non-degenerate frequency components as

$$A_i = \{(m,n,k) : [m-n+k] = i \text{ and } [m \neq n \text{ or } k \neq n]\}, \quad (20)$$

and rewrite (19) as

$$Q(z,f) = jf_0^{\frac{3}{2}}\sum_{\forall i}\delta(f-f_i)\sum_{\forall(m,n,k)\in A_i}\xi_m\xi_n^*\xi_k\sqrt{G_{\mathrm{Tx}}(f_m)G_{\mathrm{Tx}}(f_n)G_{\mathrm{Tx}}(f_k)}\,e^{\Gamma(z,f_m)+\Gamma^*(z,f_n)+\Gamma(z,f_k)}. \quad (21)$$

Inserting (21) in (17) yields the first-order solution as

$$E^{(1)}(z,f) = jf_0^{\frac{3}{2}}e^{\Gamma(z,f)}\sum_{\forall i}\delta(f-f_i)\sum_{\forall(m,n,k)\in A_i}\xi_m\xi_n^*\xi_k\sqrt{G_{\mathrm{Tx}}(f_m)G_{\mathrm{Tx}}(f_n)G_{\mathrm{Tx}}(f_k)}\int_0^z d\zeta\; e^{\Gamma(\zeta,f_m)+\Gamma^*(\zeta,f_n)+\Gamma(\zeta,f_k)-\Gamma(\zeta,f_m-f_n+f_k)}. \quad (22)$$

In order to obtain the nonlinear interference power, we compute the average PSD of the first-order solution $\gamma E^{(1)}(z, f)$. Similar to [63, Ch. IV.D], the average PSD of (22) multiplied by γ is

$$G_{\mathrm{NLI}}(z,f) = 2\gamma^2 f_0^3 e^{2\mathrm{Re}[\Gamma(z,f)]}\sum_{\forall i}\delta(f-f_i)\sum_{\forall(m,n,k)\in A_i}G_{\mathrm{Tx}}(f_m)G_{\mathrm{Tx}}(f_n)G_{\mathrm{Tx}}(f_k)\left|\int_0^z d\zeta\; e^{\Gamma(\zeta,f_m)+\Gamma^*(\zeta,f_n)+\Gamma(\zeta,f_k)-\Gamma(\zeta,f_m-f_n+f_k)}\right|^2. \quad (23)$$

In the following, we transform the inner summation appearing in (23) into a summation over two independent variables. For

the non-degenerate set A_i, we have that $f_m - f_n + f_k = f_i$ and for a given frequency triplet (f_i, f_m, f_k) it follows that $f_n = f_m + f_k - f_i$. Therefore, (23) can be written as

$$G(z, f) = 2\gamma^2 f_0^3 e^{2\mathrm{Re}[\Gamma(z,f)]} \sum_{\forall i} \delta(f - f_i) \sum_{\forall m} \sum_{\forall k} G_{\mathrm{Tx}}(f_m) G_{\mathrm{Tx}}(f_k) G_{\mathrm{Tx}}(f_m + f_k - f) \left| \int_0^z d\zeta \; e^{\Gamma(\zeta, f_m) + \Gamma^*(\zeta, f_m + f_k - f) + \Gamma(\zeta, f_k) - \Gamma(\zeta, f)} \right|^2. \quad (24)$$

Finally, we define the normalized signal power profile of a frequency component as $\rho(z, f) = e^{\int_0^z g(\zeta, f) d\zeta}$ and rewrite (24) as an integral expression by letting $f_0 \to 0$

$$G(z, f) = 2\gamma^2 \rho(z, f) \int df_1 \int df_2 \; G_{\mathrm{Tx}}(f_1) G_{\mathrm{Tx}}(f_2) G_{\mathrm{Tx}}(f_1 + f_2 - f) \left| \int_0^z d\zeta \sqrt{\frac{\rho(\zeta, f_1)\rho(\zeta, f_2)\rho(\zeta, f_1 + f_2 - f)}{\rho(\zeta, f)}} e^{j\phi(f_1, f_2, f, \zeta)} \right|^2. \quad (25)$$

As (25) was derived for single polarization, $2\gamma^2$ must be replaced by $\frac{16}{27}\gamma^2$ to obtain the nonlinear interference power for dual polarization. Furthermore, the term $\rho(z, f)$ outside of the integral can be removed when each frequency is amplified corresponding to its respective loss at the receiver. In practice, this can be realized with the use of adaptive gain flattening filters. The result is (4).

Acknowledgment

The author would like to express sincere gratitude to Dr. T. Fehenberger from Technical University of Munich for fruitful discussions on the GN model derivation. Moreover, the authors thank G. Saavedra from University College London for valuable feedback on previous drafts of the paper and Dr. D. Lavery from University College London for help with the simulation environment.

References

[1] T. Hasegawa, Y. Yamamoto, and M. Hirano, "Optimal fiber design for large capacity long haul coherent transmission," *Opt. Express*, vol. 25, no. 2, pp. 706–712, Jan. 2017.

[2] D. Semrau *et al.*, "Achievable information rates estimates in optically amplified transmission systems using nonlinearity compensation and probabilistic shaping," *Opt. Lett.*, vol. 42, no. 1, pp. 121–124, Dec. 2016.

[3] N. A. Shevchenko *et al.*, "Achievable information rates estimation for 100-nm Raman-amplified optical transmission system," in *Proc. 42nd Eur. Conf. Opt. Commun.*, Sep. 2016, pp. 1–3.

[4] G. Bosco, P. Poggiolini, A. Carena, V. Curri, and F. Forghieri, "Analytical results on channel capacity in uncompensated optical links with coherent detection," *Opt. Express*, vol. 19, no. 26, pp. B440–B451, Dec. 2011.

[5] V. Anagnostopoulos, C. T. Politi, C. Matrakidis, and A. Stavdas, "Physical layer impairment aware wavelength routing algorithms based on analytically calculated constraints," *Opt. Commun.*, vol. 270, no. 2, pp. 247–254, 2007.

[6] G. Saavedra *et al.*, "Experimental analysis of nonlinear impairments in fibre optic transmission systems up to 7.3 THz," *J. Lightw. Technol.*, vol. 35, no. 21, pp. 4809–4816, Nov. 2017.

[7] A. Nespola *et al.*, "GN-Model validation over seven fiber types in uncompensated PM-16QAM Nyquist-WDM links," *IEEE Photon. Technol. Lett.*, vol. 26, no. 2, pp. 206–209, Jan. 2014.

[8] A. Nespola *et al.*, "Experimental validation of the EGN-model in uncompensated optical links," in *Proc. Opt. Fiber Commun. Conf. Optical Society of America*, 2015, p. Th4D.2.

[9] L. Galdino *et al.*, "Experimental demonstration of modulation-dependent nonlinear interference in optical fibre communication," in *Proc. 42nd Eur. Conf. Opt. Commun.*, Sep. 2016, pp. 1–3.

[10] P. Poggiolini, G. Bosco, A. Carena, V. Curri, Y. Jiang, and F. Forghieri, "A simple and effective closed-form GN model correction formula accounting for signal non-Gaussian distribution," *J. Lightw. Technol.*, vol. 33, no. 2, pp. 459–473, Jan. 2015.

[11] D. Semrau, G. Saavedra, D. Lavery, R. I. Killey, and P. Bayvel, "A closed-form expression to evaluate nonlinear interference in Raman-amplified links," *J. Lightw. Technol.*, vol. 35, no. 19, pp. 4316–4328, Oct. 2017.

[12] A. Splett, C. Kurtzke, and K. Petermann, "Ultimate transmission capacity of amplified optical fiber communication systems taking into account fiber nonlinearities," in *Proc. Eur. Conf. Opt. Commun.*, 1993, pp. 41–44.

[13] J. Tang, "The channel capacity of a multispan DWDM system employing dispersive nonlinear optical fibers and an ideal coherent optical receiver," *J. Lightw. Technol.*, vol. 20, no. 7, pp. 1095–1101, Jul. 2002.

[14] P. Poggiolini, "The GN model of non-linear propagation in uncompensated coherent optical systems," *J. Lightw. Technol.*, vol. 30, no. 24, pp. 3857–3879, Dec. 2012.

[15] X. Chen and W. Shieh, "Closed-form expressions for nonlinear transmission performance of densely spaced coherent optical OFDM systems," *Opt. Express*, vol. 18, no. 18, pp. 19 039–19 054, Aug. 2010.

[16] P. Johannisson and M. Karlsson, "Perturbation analysis of nonlinear propagation in a strongly dispersive optical communication system," *J. Lightw. Technol.*, vol. 31, no. 8, pp. 1273–1282, Apr. 2013.

[17] A. Mecozzi and R.-J. Essiambre, "Nonlinear shannon limit in pseudolinear coherent systems," *J. Lightw. Technol.*, vol. 30, no. 12, pp. 2011–2024, Jun. 2012.

[18] M. Secondini and E. Forestieri, "Analytical fiber-optic channel model in the presence of cross-phase modulation," *IEEE Photon. Technol. Lett.*, vol. 24, no. 22, pp. 2016–2019, Nov. 2012.

[19] R. Dar, M. Feder, A. Mecozzi, and M. Shtaif, "Properties of nonlinear noise in long, dispersion-uncompensated fiber links," *Opt. Express*, vol. 21, no. 22, p. 25685, Oct. 2013.

[20] A. Carena, G. Bosco, V. Curri, Y. Jiang, P. Poggiolini, and F. Forghieri, "EGN model of non-linear fiber propagation," *Opt. Express*, vol. 22, no. 13, pp. 16335–16362, Jun. 2014.

[21] O. Golani, R. Dar, M. Feder, A. Mecozzi, and M. Shtaif, "Modeling the bit-error-rate performance of nonlinear fiber-optic systems," *J. Lightw. Technol.*, vol. 34, no. 15, pp. 3482–3489, Aug. 2016.

[22] P. Serena and A. Bononi, "A time-domain extended Gaussian noise model," *J. Lightw. Technol.*, vol. 33, no. 7, pp. 1459–1472, Apr. 2015.

[23] A. Ghazisaeidi, "A theory of nonlinear interactions between signal and amplified spontaneous emission noise in coherent wavelength division multiplexed systems," *J. Lightw. Technol.*, vol. 35, no. 23, pp. 5150–5175, Dec. 2017.

[24] A. Carena, V. Curri, G. Bosco, P. Poggiolini, and F. Forghieri, "Modeling of the impact of nonlinear propagation effects in uncompensated optical coherent transmission links," *J. Lightw. Technol.*, vol. 30, no. 10, pp. 1524–1539, May 2012.

[25] W. Shieh, H. Bao, and Y. Tang, "Coherent optical OFDM: Theory and design," *Opt. Express*, vol. 16, no. 2, pp. 841–859, Jan. 2008.

[26] A. Bononi and P. S. N. Rossi, "Performance dependence on channel baud-rate of coherent single-carrier WDM systems," in *Proc. 39th Eur. Conf. Exhib. Opt. Commun.*, Sep. 2013, pp. 1–3.

[27] L. B. Du and A. J. Lowery, "Optimizing the subcarrier granularity of coherent optical communications systems," *Opt. Express*, vol. 19, no. 9, pp. 8079–8084, Apr. 2011.

[28] Q. Zhuge, B. Chtelain, and D. V. Plant, "Comparison of intra-channel nonlinearity tolerance between reduced-guard-interval CO-OFDM systems and Nyquist single carrier systems," in *Proc. Opt. Fiber Commun. Conf. Expo. Nat. Fiber Opt. Eng. Conf.*, Mar. 2012, pp. 1–3.

[29] P. Poggiolini *et al.*, "Analytical and experimental results on system maximum reach increase through symbol rate optimization," *J. Lightw. Technol.*, vol. 34, no. 8, pp. 1872–1885, Apr. 2016.

[30] R. Dar, M. Feder, A. Mecozzi, and M. Shtaif, "Accumulation of nonlinear interference noise in fiber-optic systems," *Opt. Express*, vol. 22, no. 12, pp. 14 199–14 211, Jun. 2014.

[31] E. Agrell, A. Alvarado, G. Durisi, and M. Karlsson, "Capacity of a nonlinear optical channel with finite memory," *J. Lightw. Technol.*, vol. 32, no. 16, pp. 2862–2876, Aug. 2014.
[32] R. Dar, M. Feder, A. Mecozzi, and M. Shtaif, "Inter-channel nonlinear interference noise in WDM systems: Modeling and mitigation," *J. Lightw. Technol.*, vol. 33, no. 5, pp. 1044–1053, Mar. 2015.
[33] P. Poggiolini and Y. Jiang, "Recent advances in the modeling of the impact of nonlinear fiber propagation effects on uncompensated coherent transmission systems," *J. Lightw. Technol.*, vol. 35, no. 3, pp. 458–480, Feb. 2017.
[34] T. Fehenberger, A. Alvarado, G. Böcherer, and N. Hanik, "On probabilistic shaping of quadrature amplitude modulation for the nonlinear fiber channel," *J. Lightw. Technol.*, vol. 34, no. 21, pp. 5063–5073, Nov. 2016.
[35] G. Saavedra *et al.*, "Experimental investigation of nonlinear signal distortions in ultra-wideband transmission systems," in *Proc. Opt. Fiber Commun. Conf. Exhib.*, Mar. 2017, pp. 1–3.
[36] F. Forghieri, R. W. Tkach, and A. R. Chraplyvy, "Effect of modulation statistics on Raman crosstalk in WDM systems," *IEEE Photon. Technol. Lett.*, vol. 7, no. 1, pp. 101–103, Jan. 1995.
[37] K.-P. Ho, "Statistical properties of stimulated Raman crosstalk in WDM systems," *J. Lightw. Technol.*, vol. 18, no. 7, pp. 915–921, Jul. 2000.
[38] S. Norimatsu and T. Yamamoto, "Waveform distortion due to stimulated Raman scattering in wide-band WDM transmission systems," *J. Lightw. Technol.*, vol. 19, no. 2, pp. 159–171, Feb. 2001.
[39] E. M. Dianov, "Amplification in extended transmission bands using bismuth-doped optical fibers," *J. Lightw. Technol.*, vol. 31, no. 4, pp. 681–688, Feb. 2013.
[40] J. R. *et al.*, "First 100-nm continuous-band WDM transmission system with 115 Tb/s transport over 100km using novel ultra-wideband semiconductor optical amplifiers," in *Proc. Euro. Conf. Opt. Commun.*, 2017, pp. 1–3.
[41] E. Agrell *et al.*, "Roadmap of optical communications," *J. Opt.*, vol. 18, no. 6, 2016, Art no. 063002.
[42] D. Semrau, R. Killey, and P. Bayvel, "Achievable rate degradation of ultra-wideband coherent fiber communication systems due to stimulated Raman scattering," *Opt. Express*, vol. 25, no. 12, pp. 13 024–13 034, Jun. 2017.
[43] I. Roberts, J. M. Kahn, J. Harley, and D. W. Boertjes, "Channel power optimization of WDM systems following Gaussian noise nonlinearity model in presence of stimulated Raman scattering," *J. Lightw. Technol.*, vol. 35, no. 23, pp. 5237–5249, Dec. 2017.
[44] M. Cantono, D. Pilori, A. Ferrari, and V. Curri, "Introducing the generalized GN-model for nonlinear interference generation including space/frequency variations of loss/gain," ArXiv e-prints, 2017.
[45] M. Cantono, J. L. Auge, and V. Curri, "Modelling the impact of SRS on NLI generation in commercial equipment: an experimental investigation," in *Proc. Opt. Fiber Commun. Conf. Opt. Soc. Amer.*, 2018, p. M1D.2.
[46] J. X. Cai *et al.*, "49.3 Tb/s transmission over 9100 km using C + L EDFA and 54 Tb/s transmission over 9150 km using hybrid-Raman EDFA," *J. Lightw. Technol.*, vol. 33, no. 13, pp. 2724–2734, Jul. 2015.
[47] D. G. Foursa *et al.*, "2.56 Tb/s (256 × 10 Gb/s) transmission over 11,000 km using hybrid Raman/EDFAs with 80 nm of continuous bandwidth," in *Proc. Opt. Fiber Commun. Conf. Opt. Soc. Amer.*, 2002, p. FC3.
[48] A. N. Pilipetskii, "High-capacity undersea long-haul systems," *J. Sel. Topics Quantum Electron.*, vol. 12, no. 4, pp. 484–496, Jul. 2006.
[49] V. E. Perlin and H. G. Winful, "Optimal design of flat-gain wide-band fiber Raman amplifiers," *J. Lightw. Technol.*, vol. 20, no. 2, pp. 250–254, Feb. 2002.
[50] M. Cantono *et al.*, "On the interplay of nonlinear interference generation with stimulated Raman scattering for QoT estimation," *J. Lightw. Technol.*, to be published.
[51] I. Roberts, J. M. Kahn, J. Harley, and D. Boertjes, "Corrections to "Channel power optimization of WDM systems following Gaussian noise nonlinearity model in presence of stimulated Raman scattering"," *J. Lightw. Technol.*, vol. 36, no. 11, pp. 2309–2309, Jun. 2018.
[52] D. Semrau and P. Bayvel, "The Gaussian noise model in the presence of inter-channel stimulated Raman scattering," *arXiv:1801.02460*, 2017.
[53] G. Saavedra *et al.*, "Inter-channel stimulated Raman scattering and its impact in wideband transmission systems," in *Proc. Opt. Fiber Commun. Conf. Opt. Soc. Amer.*, 2018, p. Th1C.3.
[54] K. Minoguchi *et al.*, "Experiments on stimulated Raman scattering in S- and L-bands 16-QAM signals for ultra-wideband coherent WDM systems," in *Proc. Opt. Fiber Commun. Conf. Opt. Soc. Amer.*, 2018, p. Th1C.4.
[55] M. Tan *et al.*, "RIN mitigation and transmission performance enhancement with forward broadband pump," *IEEE Photon. Technol. Lett.*, vol. 30, no. 3, pp. 254–257, Feb. 2018.
[56] S. Tariq and J. C. Palais, "A computer model of non-dispersion-limited stimulated Raman scattering in optical fiber multiple-channel communications," *J. Lightw. Technol.*, vol. 11, no. 12, pp. 1914–1924, Dec. 1993.
[57] J. Bromage, "Raman amplification for fiber communications systems," *J. Lightw. Technol.*, vol. 22, no. 1, pp. 79–93, Jan. 2004.
[58] OFS Fitel, "TrueWave REACH optical fiber," 2014. [Online]. Available: http://fiber-optic-catalog.ofsoptics.com/Asset/TrueWaveREACHFiber-124-w eb.pdf. Accessed on: Dec. 31, 2014.
[59] P. Poggiolini, A. Carena, V. Curri, G. Bosco, and F. Forghieri, "Analytical modeling of nonlinear propagation in uncompensated optical transmission links," *IEEE Photon. Technol. Lett.*, vol. 23, no. 11, pp. 742–744, Jun. 2011.
[60] M. Zirngibl, "Analytical model of Raman gain effects in massive wavelength division multiplexed transmission systems," *Electron. Lett.*, vol. 34, no. 8, pp. 789–790, Apr. 1998.
[61] R. H. Stolen and E. P. Ippen, "Raman gain in glass optical waveguides," *App. Phys. Lett.*, vol. 22, no. 6, pp. 276–278, 1973.
[62] G. Agrawal, *Nonlinear Fiber Optics*. Amsterdam, The Netherlands: Elsevier, 2012.
[63] P. Poggiolini, G. Bosco, A. Carena, V. Curri, Y. Jiang, and F. Forghieri, "A detailed analytical derivation of the GN model of non-linear interference in coherent optical transmission systems," *ArXiv e-prints*, 2012.

Daniel Semrau (S'16) received the B.Sc. degree in electrical engineering from the Technical University of Berlin, Berlin, Germany, in 2013, the M.Sc. degree in photonic networks engineering from Scuola Superiore Sant'Anna, Pisa, Italy, and Aston University, Birmingham, U.K., in 2015. In 2015, he joined the Optical Networks Group, University College London, U.K., where he is currently working toward the Ph.D. degree. His research interests are mainly focused on channel modeling, nonlinear compensation techniques, and ultrawideband transmission for long-haul coherent optical communications.

Robert I. Killey (SM'17) received the B.Eng. degree in electronic and communications engineering from the University of Bristol, Bristol, U.K., in 1992, the M.Sc. degree from University College London (UCL), London, U.K., in 1994, and the D.Phil. degree from the University of Oxford, Oxford, U.K., in 1998. He is currently a Reader in optical communications with the Optical Networks Group with UCL. His research interests include nonlinear fiber effects in WDM transmission, advanced modulation formats, and digital signal processing for optical communications. He has participated in many European projects, including ePhoton/ONe, Nobel, BONE and ASTRON, and national projects. He is currently a Principal Investigator in the EPSRC funded UNLOC project. He was with the technical program committees of many international conferences including European Conference on Optical Communication, Optical Fiber Communication Conference ACP, and OECC. He was an Associate Editor of the IEEE/OSA JOURNAL OF OPTICAL COMMUNICATIONS AND NETWORKING and is currently an Associate Editor of the JOURNAL OF LIGHTWAVE TECHNOLOGY.

Polina Bayvel (F'10) received the B.Sc. (Eng.) and Ph.D. degrees in electronic and electrical engineering from University College London (UCL), London, U.K., in 1986 and 1990, respectively. Her Ph.D. research focused on nonlinear fiber optics and their applications. In 1990, she was with the Fiber Optics Laboratory, General Physics Institute, Moscow (Russian Academy of Sciences), under the Royal Society Postdoctoral Exchange Fellowship. She was a Principal Systems Engineer with STC Submarine Systems, Ltd., London, U.K., and Nortel Networks (Harlow, U.K., and Ottawa, ON, Canada), where she was involved in the design and planning of optical fiber transmission networks. During 1994–2004, she held a Royal Society University Research Fellowship with UCL, and, in 2002, she became a Chair in Optical Communications and Networks. She is currently the Head of the Optical Networks Group, UCL. She has authored or coauthored more than 290 refereed journal and conference papers. Her research interests include optical networks, high-speed optical transmission, and the study and mitigation of fiber nonlinearities.

Prof. Payvel was the 2002 recipient of the Institute of Physics Paterson Prize and Medal for contributions to research on the fundamental aspects of nonlinear optics and their applications in optical communications systems. In 2007, she was the recipient of the Royal Society Wolfson Research Merit Award. He is a Fellow of the Royal Academy of Engineering (F.R.Eng.), the Optical Society of America, the U.K. Institute of Physics, and the Institute of Engineering and Technology. She is a Member of the Technical Program Committee (TPC) of a number of conferences, including Proceedings of European Conference on Optical Communication (ECOC) and Co-Chair of the TPC for ECOC 2005.